Structural and magnetic properties of $FeF_2(001)/ZnF_2(001)$ and $FeF_2(110)/ZnF_2(110)$ superlattices

2003 J. Phys.: Condens. Matter 15 1201

(http://iopscience.iop.org/0953-8984/15/8/305)

INSTITUTE OF PHYSICS PUBLISHING JOURNAL OF PHYSICS: CONDENSED MATTER

J. Phys.: Condens. Matter **15** (2003) 1201–1215 PII: S0953-8984(03)52173-7

Structural and magnetic properties of $FeF_2(001)/ZnF_2(001)$ and $FeF_2(110)/ZnF_2(110)$ superlattices

Hiroki Yamazaki and Junko Satooka[1]

Magnetic Materials Laboratory, RIKEN (The Institute of Physical and Chemical Research), Wako, Saitama 351-0198, Japan

Received 9 August 2001
Published 17 February 2003
Online at stacks.iop.org/JPhysCM/15/1201

Abstract

Using the molecular beam epitaxy technique, fluoride superlattices of $FeF_2(001)/ZnF_2(001)$ and $FeF_2(110)/ZnF_2(110)$ were prepared on single-crystal substrates, $Al_2O_3(10\bar{1}0)$ and MgO(100), respectively. In addition to structural characterization, dependence of the Néel temperature on the thickness of the $FeF_2(001)$ and (110) layers was investigated in detail. The observed periodic variations of the Néel temperature with a period of 1 atomic monolayer were discussed in terms of an interface-topographical frustration due to the competing exchange interactions of J_2 and J_3.

1. Introduction

For the last several decades, a magnetic insulator FeF_2 has been investigated as a model of the three-dimensional (3D) Ising antiferromagnet. To begin with, its structural and magnetic properties are summarized below. Forming a body-centred tetragonal lattice with the Fe^{2+} ions, FeF_2 has the rutile-type crystal structure $D_{4h}^{14}-P4/mnm$ [1, 2]. A schematic diagram of the crystal structure is shown in figure 1. The Fe^{2+} free ion has a $3d^6$ configuration and the ground state is ^5D. Each Fe^{2+} ion is surrounded by six F^- ions forming an octahedron. Spin–orbit effects are adequately treated by perturbation methods, and the effective Hamiltonian pertaining to the lowest orbital state of a single Fe^{2+} ion is given by $H_s = -D\{S_z^2 - S(S+1)/3\} + E(S_x^2 - S_y^2)$ for $S = 2$, where the z axis is taken parallel to the crystalline c axis, and D and E are the uniaxial and orthorhombic anisotropy constants, respectively. Guggenheim *et al* [3] estimated $D = 6.46\ \mathrm{cm}^{-1}$ (=9.29 K) by means of inelastic neutron scattering in bulk FeF_2. Tinkham [4] obtained a result of $E \sim 0.1D$ using paramagnetic resonance and magnetic susceptibility measurements of the Fe^{2+} ions present substitutionally in a ZnF_2 lattice. Due to this strong single-ion anisotropy, FeF_2 is regarded as an Ising system. The Mössbauer spectroscopy of bulk FeF_2 also showed that the spins are aligned along the

[1] Present address: Echtechnology System Laboratory, Yokohama National University, Hodogaya, Yokohama, Kanagawa 240-8501, Japan.

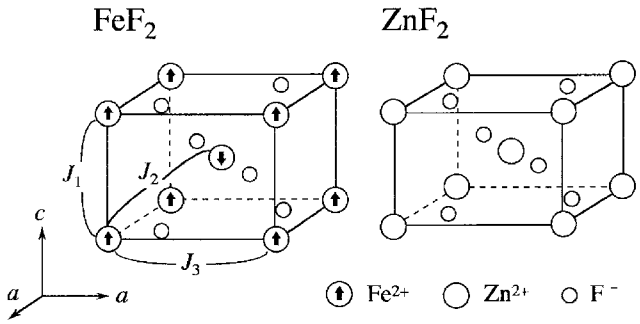

Figure 1. Crystal structures of bulk FeF_2 and ZnF_2 and spin structure of Fe^{2+} ions. The exchange interactions between the nearest (J_1), next-nearest (J_2) and third-nearest (J_3) neighbour Fe^{2+} ions are also shown.

crystalline c axis without any transverse components [5]. Magnetic interactions between the spins are the superexchange interactions via F^- ions. The exchange constants have been determined from inelastic neutron scattering [6]: $J_1 = 0.035 \pm 0.043$ K, $J_2 = -2.62 \pm 0.07$ K and $J_3 = -0.140 \pm 0.043$ K for the Hamiltonian describing the exchange interaction expressed as $H_{ex} = -2 \sum J_{ij} S_i S_j$, where the exchange constants J_1, J_2 and J_3 correspond to the exchange interactions between the nearest, next-nearest and third-nearest neighbour Fe^{2+} ions, respectively (see figure 1). Because of the dominant antiferromagnetic interaction J_2, the spins are aligned ferromagnetically in the (001) plane (c plane) and antiferromagnetically between the planes. The spin structure is also given in figure 1. Thus, FeF_2 is regarded as a simple two-sublattice antiferromagnet. A long-range antiferromagnetic ordering occurs below the Néel temperature of $T_N = 78.4$ K [1]. Intriguing subjects on FeF_2 concerning its magnetic property as an Ising antiferromagnet are the random-exchange and random-field Ising models realized in the dilute antiferromagnet $Fe_xZn_{1-x}F_2$, which has been studied extensively over the last two decades. For $x > 0.4$, the dilute antiferromagnet is an ideal example of the random-exchange Ising model when a magnetic field is not applied; and it becomes a prototypical example of the random-field Ising model when a magnetic field is applied along the magnetic easy direction [7]. For concentrations close to and below the percolation threshold $x_p \sim 0.246$ [8, 9], $Fe_xZn_{1-x}F_2$ shows a cluster-glass behaviour [10–12].

Preparing thin films of FeF_2 is promising in developing studies on this Ising antiferromagnet. From the spin structure, it is expected that the FeF_2 films can be quasi-2D Ising antiferromagnets. Using these thin films in which spins are localized to magnetic ions and are interacting with extremely short-range interactions, we can study the dependence of magnetic properties on the film thickness in terms of dimensional crossover phenomena from 3D to 2D. When the thickness is reduced to 1 atomic monolayer (ML), we obtain a 2D Ising system ideally. The FeF_2(001) films, for example, are further expected to exhibit an effect of the competing interactions of J_2 and J_3. The spin structure of bulk FeF_2 suggests that the spins on the same (001) plane, in spite of the antiferromagnetic interaction J_3 between them, are forced to align ferromagnetically by the next-nearest-neighbour spins on the adjacent (001) planes, because the intensity of J_2 is approximately 20 times as large as that of J_3. In the FeF_2 films, however, the influence of J_3 becomes distinct for the spins at the surface of the film because they have less next-nearest-neighbour spins than those inside the film. As the thickness of the FeF_2(001) film decreases, the surface effect dominates the entire film and the interactions of J_2 and J_3 become competing with respect to the ferromagnetic and antiferromagnetic alignment of the spins. For 1 ML, finally, the spins on the (001) plane are expected to align antiferromagnetically due to the unique antiferromagnetic interaction J_3.

A single FeF_2 film with a thickness of several atomic monolayers properly does not have a sufficient signal intensity that can be detected by magnetization measurements even if we use a sensitive SQUID magnetometer. Fabrication of the superlattices composed of FeF_2 and ZnF_2 layers is a solution to the problem. The nonmagnetic insulator ZnF_2 layers play the role of a structural template in the epitaxial growth of FeF_2 layers and isolate each layer of FeF_2 with respect to magnetic interactions. Both FeF_2 and ZnF_2 have the same rutile-type structure (see figure 1) with almost the same lattice constants: $a = 4.6966$ Å (4.7034 Å) and $c = 3.3091$ Å (3.1335 Å) for $FeF_2(ZnF_2)$ with the lattice mismatches of $\Delta a/a = 0.14\%$ and $\Delta c/c = 5.3\%$. Due to the excellent lattice match, particularly in a, the FeF_2 layer grows epitaxially on the ZnF_2 layer and vice versa along the c axis almost free from the epitaxial strain at the interface. Structural and magnetic properties of fluoride superlattices have already been studied not only for the combination of FeF_2 and ZnF_2 [13–15] but also for that of FeF_2 and CoF_2 [15–18]. A point unique to our study is that we have prepared a number of samples with different thicknesses of the FeF_2 layer, from 10 to 1 ML at short intervals of 0.2–0.3 ML. In this paper, thickness is expressed in the average number of monolayers of each material. In an ideal case of the layer-by-layer growth, a layer with a non-integer thickness has an incompletely filled atomic ML at the top. Owing to the number of samples, we can extract an intrinsic behaviour as a function of thickness, eliminating the extrinsic dependence on samples. In addition to the $FeF_2(001)$ layers, we have also prepared the $FeF_2(110)$ layers in the FeF_2/ZnF_2 superlattices grown epitaxially on a MgO(100) substrate following the example of the $FeF_2(110)$ film or layer on MgO(100) substrate [19–23]. Thus we have studied two series of FeF_2 layers with different crystal orientations. From the point of view of spin direction, the $FeF_2(001)$ layers have spins which are pointing perpendicular to the sample plane and the $FeF_2(110)$ layers have spins which are lying in the sample plane and are pointing in the in-plane [001] direction.

2. Sample preparation

Sample preparation was carried out using a molecular-beam-epitaxy (MBE) machine (Eiko Co., Japan). As sample sources, FeF_2 (99.5%) and ZnF_2 (99.99%) powder reagents had been formed into disc-shaped pellets of 5 mm in diameter and 3 mm in thickness with a pressing machine. In a growth chamber with a base pressure about 10^{-9} Torr, these pellets were sublimated by an electron beam to form fluoride layers on a substrate. We used single crystals of $Al_2O_3(10\bar{1}0)$ (10×10 mm$^2 \times 0.3$ mm) and MgO(100) (10×10 mm$^2 \times 0.5$ mm) as substrates. These substrates were heat-cleaned at 750 °C (Al_2O_3) or 600 °C (MgO) for 10 min in the growth chamber before beginning sample growth. First, in order to relieve the lattice mismatch between the substrate and the superlattice, a $ZnF_2(001)$ buffer layer of 400 Å was grown on $Al_2O_3(10\bar{1}0)$ and a $ZnF_2(110)$ buffer layer of 800 Å was grown on MgO(100). Next, FeF_2 and ZnF_2 were alternately deposited typically 35–50 times to obtain the superlattices of $FeF_2(001)/ZnF_2(001)$ and $FeF_2(110)/ZnF_2(110)$. The number of repetitions of FeF_2/ZnF_2 was chosen from consideration of a signal intensity that can be detected by magnetization measurements. For the samples including the FeF_2 layers with a thickness less than 4 ML, the bilayer of FeF_2/ZnF_2 was typically repeated 50 times. The number of repetitions was, as a rule, decreased to 35 as the thickness of the FeF_2 layer was increased from 4 to 10 ML. Some of the samples were prepared with the same thicknesses of FeF_2 and ZnF_2 layers and with different numbers of bilayer repetitions. For these samples, however, we did not observe the dependence of magnetic properties on the number of repetitions within experimental accuracy. Fine streak patterns of reflection high-energy electron diffraction (RHEED), which were observed during the sample growth, showed good epitaxial layer-by-layer growth. For *in situ* rate and thickness control, a precalibrated quartz-crystal oscillator (INFICON) was used. The

calibration factors were reappraised, especially for FeF_2, taking the results of *ex situ* reflection x-ray diffraction study into consideration. From the intervals between the satellite peaks and/or the low-angle diffraction profiles, the period of the bilayer repetition t_{FeF_2/ZnF_2} ($=t_{FeF_2}+t_{ZnF_2}$), where t is the thickness of the layer concerned, was determined. For a series of samples with a constant t_{ZnF_2}, we recognized that t_{FeF_2/ZnF_2} is a linear function of t_{FeF_2} and a bias corresponds to a real thickness of the ZnF_2 layer. The real thickness of the FeF_2 layer was obtained by subtracting the real thickness of the ZnF_2 layer from t_{FeF_2/ZnF_2}. The reading of the thickness on the quartz-crystal oscillator was checked by this method. A typical rate of deposit was 0.3 ± 0.1 Å s^{-1} for FeF_2 and 1.0 ± 0.3 Å s^{-1} for ZnF_2. The substrate temperature during sample growth was maintained at 300 °C for Al_2O_3 and 400 °C for MgO. These had been found out to be the optimum temperatures in view of the structural coherence length and the crystal mosaicity of the superlattices obtained by *ex situ* x-ray diffraction study and *ex situ* atomic force microscopy (AFM). In this way, two series of samples were prepared: $Al_2O_3(10\bar{1}0)/ZnF_2(001)$ [400 Å]/{$FeF_2(001)$[*n* ML]/$ZnF_2(001)$ [*m* ML]}$_{35-50}$ and $MgO(100)/ZnF_2(110)$ [800 Å]/{$FeF_2(110)$ [*n* ML]/$ZnF_2(110)$ [*m* ML]}$_{35-50}$. The thickness of the ZnF_2 layer, *m*, was typically 30 ML (12 ML) for $ZnF_2(001)$ ($ZnF_2(110)$). The thicknesses of 30 and 12 ML for the layers of $ZnF_2(001)$ and (110) correspond to 47.0 and 39.9 Å, respectively. We chose the thicknesses of 30 and 12 ML in order to give, as far as possible, the same thickness of the ZnF_2 layer for the two series of samples on condition that both the thicknesses are close to integers in units of ångströms. Though our samples were quite stable in air, they were always handled in dry N_2 or He gas, by way of a precaution.

3. Structural characterization

Structural characterization of the samples was performed mainly by *ex situ* x-ray diffraction measurements. We used an x-ray diffractometer system (Philips MRD) equipped with a rotating anode x-ray source (MAC Science) with a beam intensity of 45 kV and 100 mA using Cu Kα_1 radiation ($\lambda = 1.540\,598$ Å) collimated with a Ge(220) four-crystal monochromator. Peaks of the $Al_2O_3(10\bar{1}0)$ substrates exhibited a full width at half-maximum (FWHM), measured in 2θ for 2θ–θ scans, of about 0.01°. Figure 2 shows typical reflection x-ray diffraction patterns when the scattering vector is perpendicular to the sample plane. It was confirmed that the superlattices on $Al_2O_3(10\bar{1}0)$ and MgO(100) are preferentially oriented parallel to the (001) and (110) planes, respectively. Satellite peaks due to the repetition of the FeF_2/ZnF_2 bilayer are observed. An extra peak at about 59° in (a) corresponds to the (002) peak of the ZnF_2 buffer layer. From the FWHM of the main peak, a structural coherence length, ξ, perpendicular to the sample plane can be estimated using the Scherrer equation [24]. The vertical coherence lengths quoted using this equation only make sense when the total sample thickness is known. We obtained the average values $\xi = 320$ and 670 Å for $FeF_2(001)/ZnF_2(001)$ and $FeF_2(110)/ZnF_2(110)$, respectively. The rocking curves of the main peaks were also obtained in ω scans. The average FWHM of the rocking curves were 0.93° and 1.36° with standard deviations, when Gaussian distribution is supposed, of 0.05° and 0.04° for $FeF_2(001)/ZnF_2(001)$ and $FeF_2(110)/ZnF_2(110)$, respectively. The somewhat large FWHM of 1.36° for $FeF_2(110)/ZnF_2(110)$ is partly due to a distribution of the direction of the crystal axis in MgO that has some crystal grains typically of 1–5 mm in diameter. Using a profile-fitting program such as SUPREX [25], we tried to reproduce the diffraction patterns for some of the samples. The full curves in figure 2 represent the calculation results fitted to the experimental data points. The results of the profile fitting indicate that the interdiffusion at the interfaces between FeF_2 and ZnF_2 is extremely small. Here we mention interdiffusion as chemical interdiffusion. In the fitting procedure, we can determine the two parameters of

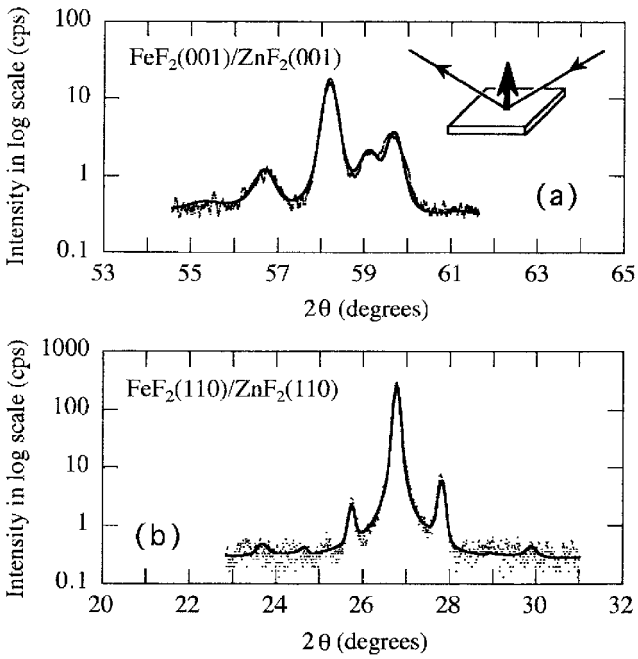

Figure 2. Typical reflection x-ray diffraction patterns of 2θ–θ scans for the scattering vector perpendicular to the sample plane for (a) $\{FeF_2(001)[10.0\ ML]/ZnF_2(001)[30\ ML]\}_{35}$ and (b) $\{FeF_2(110)[10.0\ ML]/ZnF_2(110)\ [12\ ML]\}_{35}$. The full curves correspond to the calculation results fitted to the experimental data points using the profile-fitting program SUPREX developed by Fullerton *et al* [24]. The inset shows the measurement geometry.

interdiffusion: the amount of interdiffusion and the decay length. The decay length can be larger than the thickness of one atomic plane. Chemical interdiffusion is simulated by taking a weighted average of the scattering powers of the constituent materials [25]. We set the interdiffusion parameters at zero (quite sharp interfaces) for both samples shown in figure 2. On the other hand, we took step disorder [13] into consideration. Step disorder or discrete thickness disorder assumes that the thickness is varying by an integer number of atomic planes. The effect of discrete layer thickness fluctuation is simulated by assuming a discrete Gaussian variation of the thickness about an average value [25]. In the fitting procedures, we determine σ, the width of the distribution of the thickness, for each material. For the layer of FeF_2 (ZnF_2), a typical ratio of σ/(average thickness) was 15% (17%) in $FeF_2(001)/ZnF_2(001)$ and 7% (7%) in $FeF_2(110)/ZnF_2(110)$. These values determined for $FeF_2(001)/ZnF_2(001)$ are consistent with the results obtained by Lederman *et al* [13].

In order to determine the in-plane lattice spacings directly, transmission x-ray diffraction measurements in 2θ–θ scans with the scattering vector parallel to the sample plane were carried out. The scattering geometry is shown in the inset of figure 3. Since we had not performed any special treatment to reduce the thickness of the substrate, for example by chemical etching, a time per step in the scans was set to 30 s to improve the S/N ratio of the peaks of weak intensity. We observed the (110) peak for $FeF_2(001)/ZnF_2(001)$ and the (220) and (002) peaks for $FeF_2(110)/ZnF_2(110)$. Typical diffraction patterns are shown in figure 3. For $FeF_2(001)/ZnF_2(001)$, we observed the (110) peak whose position in angle was independent of the thickness of the FeF_2 layer. For $FeF_2(110)/ZnF_2(110)$,

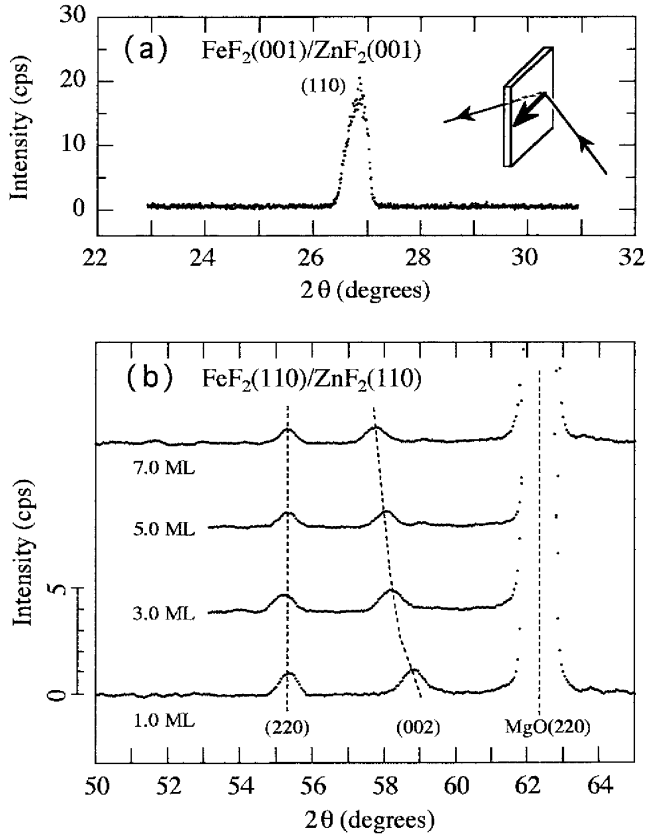

Figure 3. Typical transmission x-ray diffraction patterns of 2θ–θ scans for the scattering vector in the sample plane: (a) in-plane (110) peak for $\{FeF_2(001)[2.8\ ML]/ZnF_2(001)[16\ ML]\}_{70}$ and (b) in-plane (220) and (002) peaks for $\{FeF_2(110)[1.0–7.0\ ML]/ZnF_2(110)[12\ ML]\}_{35–50}$. The (220) peaks of MgO are from the substrate. The inset shows the measurement geometry.

the position of the (002) peak showed systematic dependence on the thickness of the FeF_2 layer, while the position of the (220) peak was almost independent of the thickness. From these peaks, the in-plane spacings were determined: d for $FeF_2(001)/ZnF_2(001)$ and $FeF_2(110)/ZnF_2(110)$ and c for $FeF_2(110)/ZnF_2(110)$, where $d(=a/\sqrt{2})$ is the lattice spacing between the (110) atomic planes and c is twice the spacing between the (001) atomic planes and is identical to the lattice constant c. Figure 4 shows the dependence of d and c on the thickness of the FeF_2 layer. Irrespective of the thickness, the in-plane spacing d's for both $FeF_2(001)/ZnF_2(001)$ and $FeF_2(110)/ZnF_2(110)$ are equal to the bulk values ($d = 3.3213$ Å for FeF_2 and $d = 3.3258$ Å for ZnF_2) within experimental accuracy. The in-plane spacing c for $FeF_2(110)/ZnF_2(110)$ falls between the bulk values ($c = 3.3091$ Å for FeF_2 and $c = 3.1335$ Å for ZnF_2) and approaches the value of ZnF_2 as the thickness decreases. The full curve in (b) indicates a calculation result fitted to the experimental data using a weighted average of the lattice constants: $c(t_1) = (c_1t_1 + c_2t_2)/(t_1 + t_2)$, where t indicates the layer thickness and the subscripts 1 and 2 denote quantities for FeF_2 and ZnF_2, respectively. The fitting procedure with a fitting parameter of c_1 was performed on condition that the in-plane spacing c_2 for ZnF_2 is equal to the bulk value (3.1335 Å). We obtained $c_1 = 3.3069 \pm 0.005$ Å which is almost equal to the bulk FeF_2 value of 3.3091 Å. This result, however, does not always

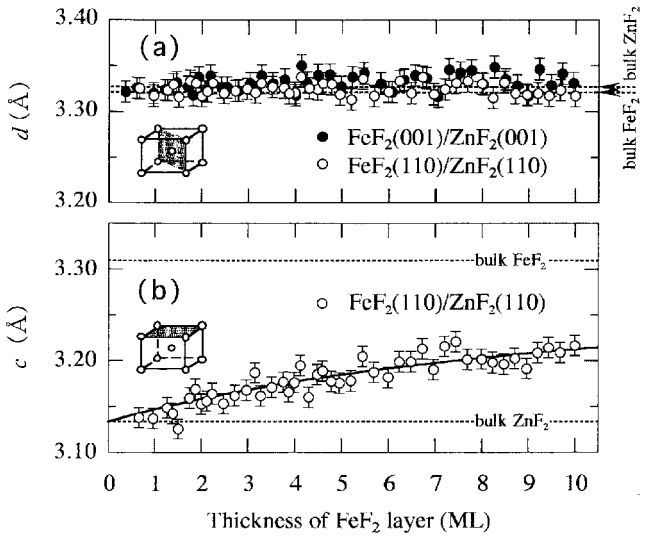

Figure 4. In-plane lattice spacings: (a) d for $FeF_2(001)/ZnF_2(001)$ and $FeF_2(110)/ZnF_2(110)$ and (b) c for $FeF_2(110)/ZnF_2(110)$, as functions of the thickness of the FeF_2 layer, where d is the lattice spacing between the (110) atomic planes (inset in (a)) and c is twice the lattice spacing between the (001) atomic planes (inset in (b)). The broken lines indicate the values of bulk FeF_2 ($d = 3.3213$ Å, $c = 3.3091$ Å) and ZnF_2 ($d = 3.3258$ Å, $c = 3.1335$ Å). The full curve in (b) represents a fit to the experimental data using a weighted average of lattice constants.

mean that the $FeF_2(110)$ layer holds the same lattice constants as bulk FeF_2 for all thicknesses. It is probable that the in-plane spacing c in the $FeF_2(110)$ layer is really contracted due to the lattice mismatch of about 5%. If so, the superlattices of $FeF_2(110)/ZnF_2(110)$ are strained only in the direction parallel to the in-plane [001], in contrast with those of $FeF_2(001)/ZnF_2(001)$ that are almost free from the in-plane lattice strain because of a good lattice match in the a axis. The contraction of the lattice spacing is supported, as we will see later, by an increase in the Néel temperature from the bulk value of 78.4 K.

The fluoride crystal orientation in the sample plane with respect to the substrate was determined from the x-ray diffraction scans in the angle ϕ around the axis perpendicular to the sample plane. During the scans, the angles of 2θ and ω were fixed under the (221) or (112) reflection Bragg condition. The inset of figure 5 shows the scattering geometry. The diffraction patterns obtained (typical ones are shown in figure 5) revealed a fourfold symmetry for $FeF_2(001)/ZnF_2(001)$ and also for $FeF_2(110)/ZnF_2(110)$. The difference in intensity for four peaks may partly come from the condition that the rotation axis deviates slightly from the real axis of [001] or [110] of the fluoride superlattices. From the observed symmetry, orientations of the FeF_2/ZnF_2 surface unit cells of (001) and (110) with respect to the substrate are shown in figure 6. The superlattices on the $Al_2O_3(10\bar{1}0)$ substrate have two orthogonal a axes on the sample plane with the relations: $Al_2O_3[0001] \parallel FeF_2/ZnF_2[100]$ and $Al_2O_3[1\bar{2}10] \parallel FeF_2/ZnF_2[010]$. The superlattices on the MgO(100) substrate are twinned in the plane because the (110) surface unit cell of the fluoride superlattices is rectangular, while the MgO(100) surface unit cell is square. The two in-plane domains are determined by $FeF_2/ZnF_2[001] \parallel MgO[110]$ and $FeF_2/ZnF_2[1\bar{1}0] \parallel MgO[1\bar{1}0]$ and its corresponding twin (the unit cell rotated by 90°). In figure 6, the spin directions expected of the Fe^{2+} ions are also shown. Due to the strong single-ion anisotropy, the spins are always pointing parallel to

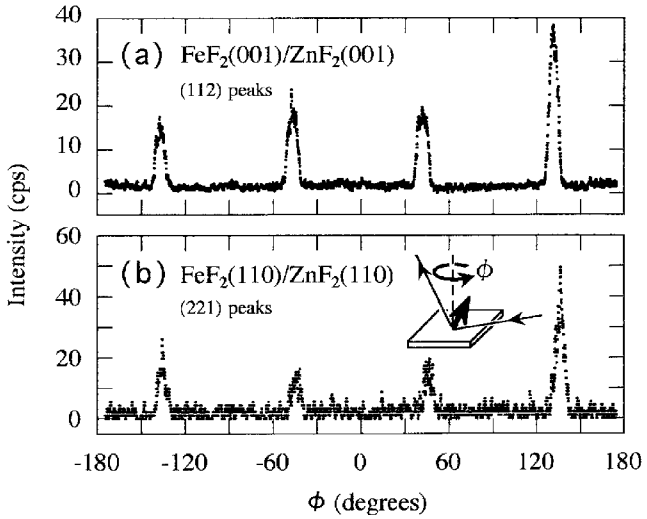

Figure 5. Typical x-ray diffraction patterns of ϕ scans for (a) $\{FeF_2(001)[10.0\ ML]/ZnF_2(001)\ [30\ ML]\}_{35}$ and (b) $\{FeF_2(110)[10.0\ ML]/ZnF_2(110)[12\ ML]\}_{35}$, where ϕ is the rotation angle around the axis perpendicular to the sample plane. Scans were carried out with the angles of 2θ and ω fixed to the (112) or (221) reflection Bragg condition. The inset shows the scattering geometry.

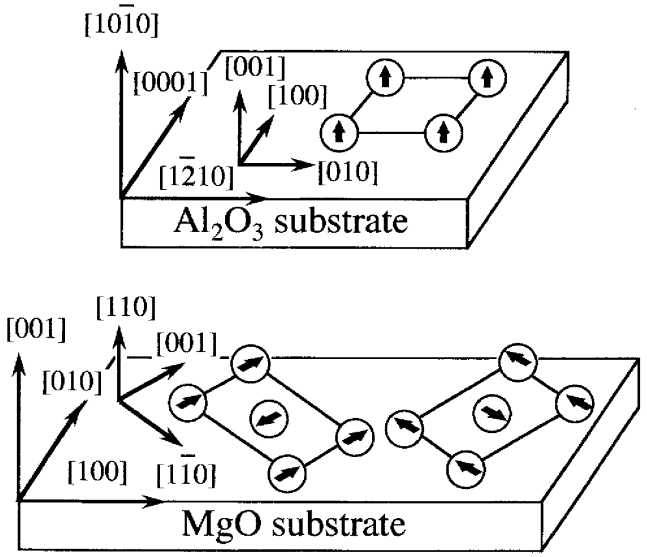

Figure 6. Orientation of the (001) and (110) surface unit cells with respect to the single-crystal substrate. The spin directions of the Fe^{2+} ions are also shown.

the *c* axis even in the case of the Fe^{2+} ions diluted in ZnF_2 [4]. In the layers of $FeF_2(110)$, therefore, two magnetic in-plane domains exist with their magnetic easy axes (*c* axis) in the plane, but perpendicular to each other.

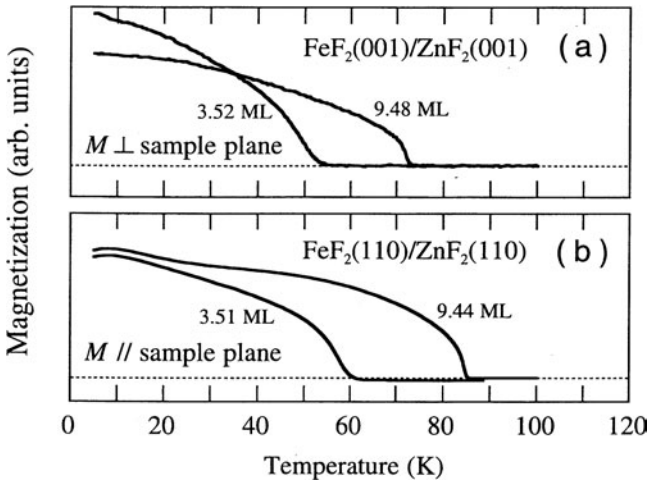

Figure 7. Typical plots of temperature dependence of remanent magnetization M_r measured for increasing temperatures without magnetic field. Measurements were performed after field cooling down to 5 K with a field of 100 Oe applied along the magnetic easy direction: (a) perpendicular to the sample plane for $FeF_2(001)/ZnF_2(001)$ and (b) parallel to the sample plane for $FeF_2(110)/ZnF_2(110)$. The figures by the curves indicate the thickness of the FeF_2 layer.

4. Magnetic properties

Magnetic properties of the samples were studied using a SQUID magnetometer (Quantum Design $MPMS_2$). Our principal interest lies in the dependence of the Néel temperature T_N on the thickness of the FeF_2 layer. In order to determine T_N for each sample, we measured a small ferromagnetic moment which remains after field cooling in a weak magnetic field. This weak-field-induced magnetization or remanent magnetization M_r, which is assumed to be of piezomagnetic origin [26–28], has been observed for the diluted bulk samples of $Fe_xZn_{1-x}F_2$ [26, 27] and also for the pure bulk sample of FeF_2 [28]. We defined T_N as the temperature at which M_r disappears on increasing temperature. It was observed that, within experimental accuracy, the Néel temperature defined as above corresponds to the temperature below which a difference in magnetization appears between the field-cooling procedure and the field-warming procedure that was performed after zero-field cooling [29]. Before starting measurements, samples were cooled down to 5 K in a magnetic field of 100 Oe. For $FeF_2(001)/ZnF_2(001)$, the direction of the magnetic field was parallel to the c axis of the superlattice (perpendicular to the sample plane). For $FeF_2(110)/ZnF_2(110)$, the magnetic field was applied parallel to the sample plane and parallel to the a axis of the MgO substrate. In this case, it is impossible to apply a magnetic field exclusively along the c axis of the superlattice due to the twinning of the $FeF_2(110)$ crystal (see figure 6). After removing a magnetic field to $|H| < 0.1$ Oe at 5 K, the remanent magnetic component parallel to the direction of the magnetic field was measured for increasing temperatures. Figure 7 shows typical plots of temperature dependence of M_r. We observed fairly sharp transitions for the thicknesses more than about 4 ML. A rounding of the transition was found for other thicknesses as we see for 3.52 ML in (a) and 3.51 ML in (b).

We direct our attention to the remanent magnetization at 5 K. Figure 8 shows the remanent magnetization M_r parallel to the c axis at 5 K for the $FeF_2(001)$ layers with a thickness of n ML, where n is an integer. The values of M_r have been reduced per single FeF_2 layer

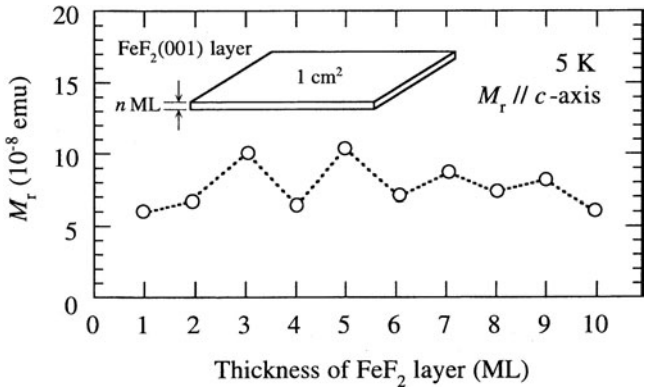

Figure 8. Remanent magnetization M_r parallel to the c axis (perpendicular to the sample plane) at 5 K as a function of the integer thickness of the $FeF_2(001)$ layer. The value of M_r has been reduced per one slab of the FeF_2 layer of 1 cm^2 in area (the inset diagram). The vertical error bars are not shown since the error in the vertical direction is within each symbol.

(not an atomic plane) of 1 cm^2 in area (see the inset of figure 8). In the figure, we recognize an inequality $M_{r(n=\text{odd})} > M_{r(n=\text{even})}$ except for $n = 1$ (ML). The spin structure of the Fe^{2+} ions (see figure 1) can clarify the dependence of M_r on the number of n. In the $FeF_2(001)$ layers with an odd number of (001) atomic planes (n = odd), we detect a ferromagnetic moment of uncompensated spins due to the alternating ferromagnetic (001) planes. For n = even, on the other hand, magnetic moments are all compensated (cancelled out) and we detect no magnetic moment. Our experimental results show that M_r are biased, probably, by the piezomagnetic moment. This type of uncompensated spins have been observed in CoO/SiO_2 multilayers, where CoO is also an antiferromagnetic insulator [30]. The exception at 1 ML in the experimental results is understandable because the spins set exclusively on a plane of (001) are aligned antiferromagnetically without composing a ferromagnetic plane due to the antiferromagnetic interaction J_3, which is the only interaction that exists between the spins. Ideally, the ferromagnetic moment of the uncompensated spins in 1 cm^2 has an identical value for all the samples of 1 cm^2 in area with n = odd because the ferromagnetic moment comes from the spins on an atomic plane in the FeF_2 layer. Calculation using $g_{\|c} = 2.25$ [31] gives a ferromagnetic moment of 1.9×10^{-5} emu. We expect that the difference $\Delta M_r = M_{r(n=\text{odd})} - M_{r(n=\text{even})}$ obtained experimentally corresponds to this ferromagnetic moment even if M_r are biased by the piezomagnetic moment. The experimental value of $\Delta M_r = 2\text{–}4 \times 10^{-8}$ emu, which can be seen in figure 8, is, however, more than two orders of magnitude smaller than the calculation value. Fluctuation of the spin component due to a frustration effect can clarify the reduction of ΔM_r from the expected value. We will discuss the frustration effect in the next section.

The behaviour of the magnetization in the critical region reflects the dimension (d_s) of the system and the number of spin components (n_s) [32, 33]. Since the spins of the Fe^{2+} ions have a strong uniaxial anisotropy, both the layers of $FeF_2(001)$ and $FeF_2(110)$ behave as a system of $n_s = 1$ in the vicinity of T_N. As the thickness of the FeF_2 layer decreases, therefore, the critical behaviour of our samples changes from that of the 3D Ising ($d_s = 3$ and $n_s = 1$) to the 2D Ising ($d_s = 2$ and $n_s = 1$). For some of the samples, we tried to determine the critical exponent β from a fit of the experimental data to the power law $M_r \propto (M_s \propto) t^{\beta}$, where M_s is the staggered magnetization (or sublattice magnetization) and t ($\equiv |T/T_N - 1|$) is the reduced temperature. It has been suggested that the staggered magnetization M_s is proportional to

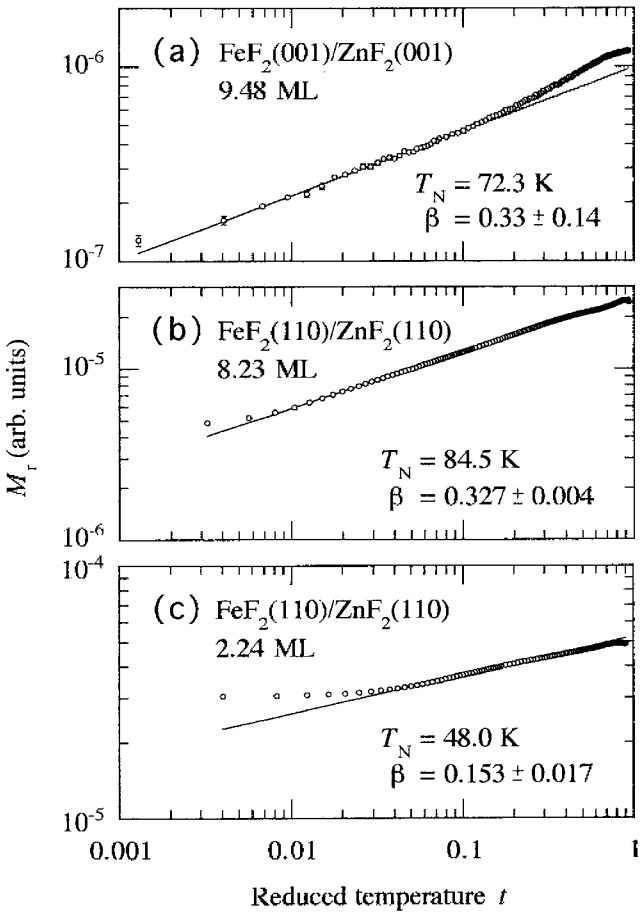

Figure 9. Log–log plots of remanent magnetization M_r as a function of the reduced temperature t ($\equiv |T/T_N - 1|$) for (a) $FeF_2(001)$[9.48 ML], (b) $FeF_2(110)$[8.23 ML] and (c) $FeF_2(110)$ [2.24 ML]. The experimental points appear to be fitted by a power law $M_r \propto t^{\beta}$. The critical exponent β obtained from the fit is shown in each panel together with the Néel temperature T_N.

the remanent magnetization M_r in the critical region [28]. Figure 9 shows the examples of the log–log plots of M_r as a function of t and the results of fitting to the power law. Due to the rounding of the transition and the reduction of T_N, we failed to carry out a fit of the data to the power law for the $FeF_2(001)$ layers with thicknesses less than about 4 ML and for the $FeF_2(110)$ layers with thicknesses less than about 2 ML. From the theoretical study, it is known that $\beta = 0.325$ and 0.125 for the 3D and 2D Ising system, respectively [32, 33]. As shown in (a) and (b) in figure 9, the critical exponents obtained for the thicker layers of $FeF_2(001)$ and $FeF_2(110)$ are almost equal to the value of the 3D Ising system. The critical exponent close to 0.325 has already been obtained for a bulk sample of FeF_2 [28] and a thin film of FeF_2 of thickness 0.8 μm [34]. Our results reveal that a film (or layer) of FeF_2 behaves like a 3D Ising system for the thicknesses down to about 10 ML. The $FeF_2(110)$ layer with a thickness of 2.24 ML in (c), on the other hand, shows a critical exponent obviously smaller than 0.325 and rather close to 0.125. This result suggests that dimensional crossover from 3D to 2D occurs as the thickness of the $FeF_2(110)$ layer decreases.

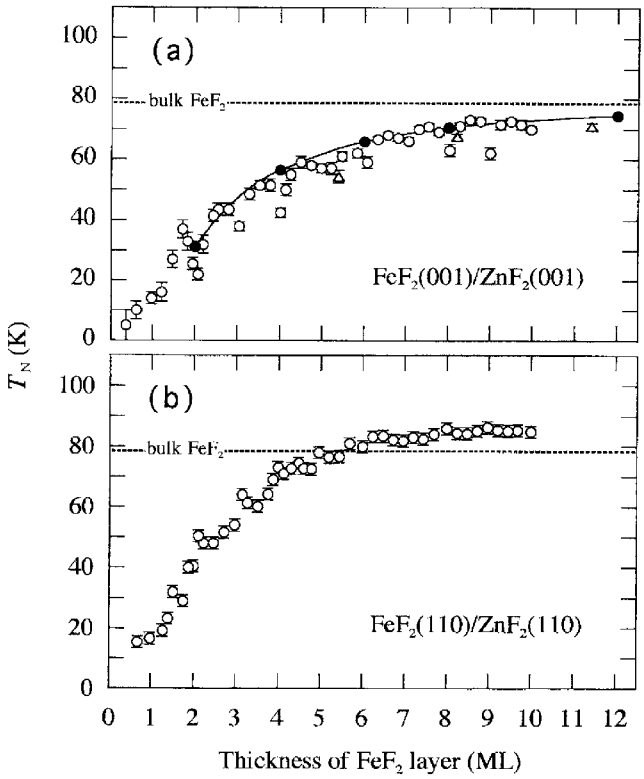

Figure 10. Dependence of the Néel temperature T_N on the thickness of the FeF_2 layer for the samples of (a) $FeF_2(001)/ZnF_2(001)$ and (b) $FeF_2(110)/ZnF_2(110)$. The broken lines indicate T_N of bulk FeF_2. In (a), results of Monte Carlo simulations [13] for the $S = 2$ Ising spins in the body-centred tetragonal lattice (•) and T_N's obtained from the thermal-expansion measurements (△) [13]. The full curve in (a) is a guide to the eyes.

The dependence of T_N on the thickness of the layers of $FeF_2(001)$ and (110) is shown in figure 10. In (a), the results of thermal-expansion measurements (open triangles) and Monte Carlo simulations (filled circles) obtained by Lederman *et al* [13] are also indicated for reference. Monte Carlo simulations were performed for the $S = 2$ Ising spins in the body-centred tetragonal lattice interacting only with the dominant interaction J_2 [13]. Since the thermal-expansion measurements were carried out for the FeF_2/ZnF_2 superlattices grown parallel to the c axis, we can immediately compare their T_N's with those for our $FeF_2(001)/ZnF_2(001)$ samples. Our results (open circles) are quite consistent with the results obtained by the thermal-expansion measurements for 5.4 and 8.2 ML. Regarding the overall behaviour, we observe that T_N decreases with decreasing the thickness for both layers of $FeF_2(001)$ and (110). Because the finite-size scaling [13, 30] is strictly valid only for T_N not far from $T_{N(bulk)}$, the dependence of T_N on the thickness cannot be reproduced by the scaling for all the thicknesses. For the $FeF_2(001)$ layers, we see that T_N as a function of thickness is reproduced well by the results of Monte Carlo simulations for those thicknesses more than 2 ML. For a guide to the eyes, the full curve in (a) is drawn by means of the extrapolation of the simulation results. We find discrepancies between the curve and the experimental data only at those thicknesses in the vicinity of integers. These discrepancies correspond to local dips of T_N. In (b), on the other hand, we observe local peaks of T_N at integer thicknesses from 2 to

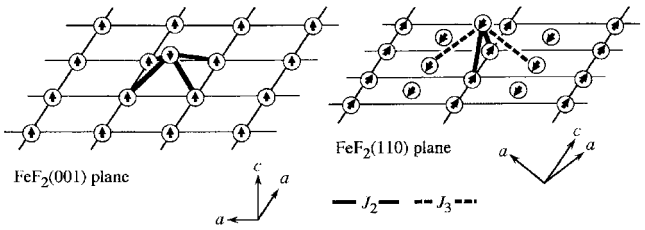

Figure 11. Spin structures of the (001) and (110) atomic planes of FeF_2. The exchange interactions between the spin of an additional Fe^{2+} ion and the spins on the plane are shown. The interactions between the spins on the plane are not indicated for clarity.

5 ML. At integer thicknesses, we recognize the deviation of T_N in opposite directions (dip or peak) according to the growth directions ((001) or (110)) of the FeF_2 layers. We will discuss the origin of the dips and peaks in the next section. It is quite confusing to find such periodic variations in T_N with a short period of 1 ML. According to the results of the profile fitting of x-ray diffraction patterns, the FeF_2 layers have step disorder, where a distribution of the thickness of the FeF_2 layer exists. If this is true, due to a concomitant distribution of T_N for a sample, the periodic variation of T_N with a short period as a function of *average* thickness should have been smeared out. It is probable that a real distribution of the FeF_2 layer thickness is not so broad as was estimated from the profile fitting of the x-ray diffraction patterns, so it is questionable whether the model used in the profile fitting is appropriate for the FeF_2/ZnF_2 superlattices. Analysis of grazing incidence, which would certainly improve the structural characterization of the samples, should be carried out in the near future. The $FeF_2(110)$ layers have T_N's which are somewhat higher than those for $FeF_2(001)$, particularly at larger thicknesses. Especially for the thicknesses more than 6 ML, they have obviously higher T_N's than the T_N of the bulk by about 10%. This is due to a small contraction of the $FeF_2(110)$ layers in the direction parallel to the in-plane [001], as was mentioned in the previous section. It is known that the interaction between the spins of Fe^{2+} ions is the superexchange interaction via F^- ions and is sensitive to a change in distance. When the distance between Fe^{2+} ions decreases due to the contraction parallel to the in-plane [001], the exchange integral increases, resulting in the increase of T_N. The results of the $FeF_2(110)$ layers reveal that we can increase T_N using the epitaxial strain at the interfaces.

5. Discussion

Regarding the discrepancy between the T_N's calculated by Monte Carlo simulations and those obtained by the thermal-expansion measurements, Lederman *et al* [13] concluded that the discrepancy has its origin in the fundamental magnetic Hamiltonian of FeF_2, which is really not Ising-like, but is instead Heisenberg-like with single-ion anisotropy. As we have seen in the previous section, however, the T_N's obtained by experimental studies deviate from those of Monte Carlo simulations only at integer thicknesses. As for structure, we do not observe any anomaly at integer thicknesses (see figure 4). Hence, supposing that the observed dips and peaks in T_N are essentially of magnetic origin, our interpretation is as follows. We have to take the interaction J_3 as well as J_2 into consideration in the magnetic Hamiltonian. It has been mentioned in section 1 that the interactions of J_2 and J_3 can become competing in the thin layers of $FeF_2(001)$ because the spins at the interfaces have less next-nearest-neighbour spins than those inside the layer. At integer thicknesses, when the top atomic plane of $FeF_2(001)$ is completely filled, a frustration effect in the top atomic plane reduces T_N of the $FeF_2(001)$

layer. When we add an Fe^{2+} ion to a site on the next ($(n+1)$th) atomic plane, this ion stabilizes a ferromagnetic alignment of the four spins on the nth plane due to the interaction J_2 (see the left diagram of figure 11). By adding more Fe^{2+} ions to the $(n+1)$th plane, the area where the ferromagnetic alignment is stabilized increases on the nth plane and T_N increases. At the thickness of $(n + p_c)$ ML, where p_c (=0.592 745 for square lattices [9]) is a percolation threshold, the Fe^{2+} ions make a percolation cluster on the $(n+1)$th plane and a frustration again begins to be exhibited in the $(n+1)$th plane, so that T_N begins to decrease, making a peak there. In this manner the degree of frustration is the highest at integer thicknesses for the $FeF_2(001)$ layer, which is the reason why T_N has local dips at integer thicknesses. We can also explain the peak of T_N just below 2 ML, correctly at 1.69 ML $\fallingdotseq (1 + p_c)$ ML, in terms of a frustration effect. At this thickness, however, we obtain a sharper peak than those at $(n + p_c)$ ML, where $n \geqslant 2$, because the change of T_N as a function of thickness is more pronounced in the thickness range between 1 and 2 ML. This is due to the fact that, in the $FeF_2(001)$ layers with thicknesses between 1 and 2 ML, the interactions J_2 and J_3 are the most competing because the Fe^{2+} ions are all on the 'surfaces' of the FeF_2 layer. The explanation in terms of a frustration effect also clarifies the reduction of ΔM_r from the expected value as we have mentioned in the previous section. In the case of the $FeF_2(110)$ layers, on the other hand, an Fe^{2+} ion added to a site on the next ($(n+1)$th) atomic plane appears to destabilize the antiferromagnetic alignment of the four spins on the nth plane (see the right diagram of figure 11). The additional spin is interacting with two spins via J_2, which prefers antiferromagnetic alignment, and with other two spins via J_3, which also prefers antiferromagnetic alignment. If $|J_2| \sim |J_3|$ holds effectively, a frustration occurs with respect to the alignment of these spins. Hence, the $FeF_2(110)$ layers exhibit the least frustration at integer thicknesses and T_N has the local peaks there. In the FeF_2 layers with a thickness of several ML's, it is probable that the exchange interactions J_1, J_2 and J_3 are effectively changed from those of bulk FeF_2 because (1) the number of the exchange paths via F^- ions is changed, especially in the vicinity of the interfaces and (2) the lattice constants are changed due to epitaxial strain. For the thickness of 1 ML, we obtained the transition temperatures of $T_N = 14 \pm 2$ K for the $FeF_2(001)$ layer and $T_N = 16.5 \pm 2$ K for the $FeF_2(110)$ layer (see figure 10). These results suggest $|J_2| \sim |J_3|$ because the transition temperature of 2D Ising spins in a square lattice is proportional to the exchange integral [35]. The $FeF_2(001)$ and (110) layers with 1 ML thickness can be regarded as the 2D Ising spins in a square lattice interacting with J_3 and with J_2, respectively, when we ignore J_1 in the $FeF_2(110)$ layer because of $|J_1| \ll |J_2|$. We have discussed the periodic variations of the Néel temperature with a period of 1 atomic ML in terms of an interface-topographical frustration effect due to the competing exchange interactions of J_2 and J_3. The above discussion is just a qualitative one. We are planning to perform Monte Carlo simulations, taking the exchange interactions of J_2 and J_3 into consideration in the magnetic Hamiltonian.

Acknowledgments

The authors thank Professor I K Schuller and Dr C Leighton for information on preparing fluoride layers using electron-beam evaporation. Thanks are also given to Dr N Nakayama (Yamaguchi University) for his useful comment on the structural characterization and to Dr K Kawaguchi (AIST) for help in performing a part of the magnetization measurements. This work was motivated by Dr K Katsumata at first. The authors have been supported by Grants-in-Aid for Scientific Research from the Ministry of Education, Culture, Sports, Science and Technology of Japan. One of the authors (JS) was supported by the Special Postdoctoral Researchers Program of RIKEN and by the Hayashi Memorial Foundation for Female Natural Scientists.

References

[1] Stout J W and Catalano E 1955 *J. Chem. Phys.* **23** 2013
[2] Stout J W and Reed S A 1954 *J. Am. Chem. Soc.* **76** 5279
[3] Guggenheim H J, Hutchings M T and Rainford B D 1968 *J. Appl. Phys.* **39** 1120
[4] Tinkham M 1956 *Proc. R. Soc.* A **236** 535
Tinkham M 1956 *Proc. R. Soc.* A **236** 549
[5] Wertheim G K 1961 *Phys. Rev.* **121** 63
[6] Hutchings M T, Rainford B D and Guggenheim H J 1970 *J. Phys. C: Solid State Phys.* **3** 307
[7] Belanger D P 1998 *Spin Glasses and Random Fields* ed A P Young (Singapore: World Scientific) and references therein
[8] Sykes M F and Essam J 1964 *Phys. Rev.* **133** A310
[9] Stauffer D and Aharony A 1994 *Introduction to Percolation Theory* (London: Taylor and Francis)
[10] Satooka J and Ito A 1997 *J. Phys. Soc. Japan* **66** 784
[11] Satooka J and Ito A 1998 *J. Phys.: Condens. Matter* **10** L711
[12] Barbosa P H R, Raposo E P and Countinho-Filho M D 2001 *Physica* A **295** 140
[13] Lederman D, Ramos C A, Jaccarino V and Cardy J L 1993 *Phys. Rev.* B **48** 8365
[14] Ramos C A, Cáceres M O and Lederman D 1996 *Phys. Rev.* B **53** 7890
[15] Jaccarino V, King A R, Lederman D, Lui M and Ramos C A 1991 *Mater. Res. Soc. Symp. Proc.* **221** 3
[16] Ramos C A, Lederman D, King A R and Jaccarino V 1990 *Phys. Rev. Lett.* **65** 2913
[17] Lederman D, Ramos C A and Jaccarino V 1993 *J. Phys.: Condens. Matter* **5** A373
[18] Lederman D, Belanger D P, Wang J, Han S-J, Paduani C, Ramos C A and Nicklow R M 1993 *Mater. Res. Soc. Symp. Proc.* **313** 333
[19] Nogués J, Lederman D, Moran T J, Schuller I K and Rao K V 1996 *Appl. Phys. Lett.* **68** 3186
[20] Nogues J, Lederman D, Moran T J and Schuller I K 1996 *Phys. Rev. Lett.* **76** 4624
[21] Adenwalla S, Felcher G P, Nogués J and Schuller I K 1997 *J. Appl. Phys.* **81** 5307
[22] Miltényi P, Gruyters M, Güntherodt G, Nogués J and Schuller I K 1999 *Phys. Rev.* B **59** 3333
[23] Nogués J, Moran T J, Lederman D, Schuller I K and Rao K V 1999 *Phys. Rev.* B **59** 6984
[24] Warren B E 1990 *X-ray Diffraction* (New York: Dover)
[25] Fullerton E E, Schuller I K, Vanderstraeten H and Bruynseraede Y 1992 *Phys. Rev.* B **45** 9292
[26] Kushauer J, Kleemann W, Mattsson J and Nordblad P 1994 *Phys. Rev.* B **49** 6346
[27] Kushauer J, Binek C and Kleemann W 1994 *J. Appl. Phys.* **75** 5856
[28] Mattsson J, Djurberg C and Nordblad P 1994 *J. Magn. Magn. Mater.* **136** L23
[29] Yamazaki H and Satooka J 2002 *J. Magn. Magn. Mater.* **240** 442
[30] Ambrose T and Chien C L 1996 *Phys. Rev. Lett.* **76** 1743
[31] Ohlmann R C and Tinkham M 1961 *Phys. Rev.* **123** 425
[32] Gebhardt W and Krey U 1980 *Phasenübergänge und Kritische Phänomene* (Friedr. Vieweg and Sohn: Braunschweig/Wiesbaden)
[33] Stanley H E 1971 *Introduction to Phase Transitions* (Oxford: Clarendon)
[34] Belanger D P, Lui M and Erwin R W 1993 *Mater. Res. Soc. Symp. Proc.* **313** 755
[35] McCoy B M and Wu T T 1973 *The Two-dimensional Ising Model* (Cambridge, MA: Harvard University Press)